electricity

MDPI

Article

Optimal Operation of Self-Healing Networked Microgrids Using Pufferfish Optimization Algorithm

Omar H. Abdalla *, Ahmed A. Abdelrazek and Mohamed H. Abdo

Department of Electrical Power and Machines Engineering, Faculty of Engineering, Capital University (Formerly, Helwan University), Cairo 11792, Egypt; ahmed.abdelrazek.24@h-eng.helwan.edu.eg (A.A.A.); drmhsa3ed@eng.capu.edu.eg (M.H.A.)

* Correspondence: omar.hanafy@eng.capu.edu.eg or omar.hanafy@h-eng.helwan.edu.eg

Abstract

This paper presents an approach for optimal operation of self-healing networked microgrids (NMGs) under both normal operation and emergency conditions using the pufferfish optimization algorithm (POA). The proposed methodology is based on an energy management system (EMS) with two levels and independent functions. The lower-level is designed for normal operation, where the local controller of each microgrid (MG) performs the optimal dispatch of power from the dispatchable sources. During an emergency case in any MG, the higher-level EMS is activated, and the global controller is brought into operation. Physically, the NMGs are connected by tie-lines, while cyber links are established to exchange information and control signals for coordinated operation. Each MG operates to supply its local demand during normal operation conditions, resulting in no electrical power exchange between MGs. İn case of generation deficiency or a fault leading to generation outage, electrical power can be exchanged through the existing interconnections, enabling the affected microgrid to receive support from neighboring MGs. The main objective of POA is to minimize the total operating cost, in which the economic impact of network power losses is incorporated into the single objective function. Simulation studies were conducted using MATLAB and DIgSILENT software over one day. The performance of POA was compared with Particle Swarm Optimization (PSO), Genetic Algorithm (GA), and Grey Wolf Optimizer (GWO) under the same computational settings. Statistical and convergence analyses show that POA achieves the lowest mean operating cost across all studied cases, with low run-to-run variability and favorable convergence behavior. The results demonstrate the effectiveness of the proposed approach in improving the economic operation of NMGs under both normal and emergency conditions.

Keywords: self-healing; networked microgrids; pufferfish optimization algorithm; energy management system

Check for updates

Academic Editor: Pedro Manuel Soares Moura

Received: 26 July 2026
Revised: 30 August 2026
Accepted: 1 September 2026
Published: 4 September 2026

Copyright: © 2026 by the authors. Licensee MDPI, Basel, Switzerland. This article is an open access article distributed under the terms and conditions of the Creative Commons Attribution (CC BY) license.

1. Introduction

A microgrid is defined as a group of distributed energy resources (DERs), including renewable energy sources (RESs) and battery energy Storage Systems (BESSs), plus loads that operate locally as a single controllable entity [1]. Connecting multiple MGs to construct networked microgrids (NMGs) represents a further development and application of the MG concept. According to the IEEE Standard 1547.4 [2], the operation and reliability of a distribution system can be improved by partitioning it into multiple MGs. Under normal operating conditions, each MG operates independently and supplies its local load.

However, during major contingencies, the limited capacity of individual MGs necessitates the formation of NMGs, which allows a coordinated exchange of power and improves the resiliency of the entire system [3]. Early research has already demonstrated that the ability to coordinate the behavior of interconnected MGs can significantly enhance their self-healing capabilities [4]. Self-healing is an advanced and active approach for operating and planning the network that can isolate the part that is affected by the contingency in an emergency and restore the system to its usual functioning [5,6]. In [7], a decentralized operation structure was suggested to facilitate the distribution of power among MGs in single and multiple faults. The concept was extended further in [8], in which an optimal self-healing operation strategy was designed to distribute the power support of healthy MGs and reduce the cost of operation. In a similar manner, authors in [9] presented a coordinated control strategy that enhances the stability of the system by allowing adaptable collaboration among interconnected MGs under abnormal operating conditions. As the complexity operation of self-healing NMGs increased, optimization-based methods attracted considerable interest. In [10], a comprehensive self-healing strategy has been proposed that considers network reconfiguration, generation redispatch, and load shedding in a unified framework under uncertainty. Moreover, consensus-based approaches to decentralization have been suggested in [11] to limit the use of centralized controllers and improve scalability in multi-microgrid settings. The mixed-integer linear programming and advanced communications infrastructures were adopted in [12] to introduce fast self-healing and service restoration schemes. Additionally, self-healing frameworks based on optimization have been created to guarantee the mutual coordination of power exchange between interconnected microgrids under fault conditions to maximize restoring load and minimize the operational costs [13]. In [14], the authors proposed a methodology for determining the optimal number and locations of smart ring main units (SRMUs) in self-healing smart distribution networks using nonlinear programming (NLP) and mixed integer linear programming (MILP) optimization techniques while considering costs related to power losses, energy not supplied (ENS) and PV disconnection. In [15], a service restoration policy was proposed based on a mixed-integer optimization strategy of NMGs that can facilitate coordinated dispatch of distributed generators and energy storage systems when self-healing. Optimization-oriented studies further extended self-healing capabilities in NMGs through coordinated scheduling and resilience-aware decision-making [16,17]. Simultaneously with mathematical optimization methods, heuristic and metaheuristic algorithms have continued to be more widely used to solve the computational complexity of self-healing and restoration problems in microgrid-based systems. The optimal economic management of microgrids with fuel cell integration was done using marine predator algorithms and achieved more cost-effectiveness than the traditional algorithms [18]. Improved heuristic optimization mechanisms, like the wind-driven one that uses crossover operations, have been used in demand response schedules in smart grids that are rich in renewable energy [19]. Bi-objective active and reactive power flow optimization in hybrid microgrids is performed using particle swarm optimization (PSO) [20]. Comprehensive survey works have documented the increased use of metaheuristics like PSO, GA, and the grey wolf optimizer to improve the performance of microgrids and restoration processes [21,22]. Recently, an improved Honey Badger Algorithm (HBA) was applied to optimize energy management in smart microgrids, achieving lower operational cost, improving system reliability, and effectively balancing generation, storage, and grid power contributions compared with Sparrow Search Algorithm (SSA), PSO, and GA [23]. Furthermore, a quantum-accelerated digital twin (QDT) framework integrating quantum optimization algorithms with a high-fidelity digital twin (DT) has been proposed for real-time detection, localization, and remediation of cyberattacks in power distribution systems [24].

Although these contributions are valuable, there are still several limitations. The majority of the existing literature assumes that microgrids are interconnected by a common bus or centralized point of connection, which constrains the ability of the microgrids to operate flexibly and impairs the autonomy of individual microgrids. Despite the deployment of diverse metaheuristic optimization methods in the operation of microgrids, their implementation for the coordinated optimal operation of NMGs under normal and emergency conditions, taking into explicit consideration energy losses, has been limited. To overcome these challenges, this paper presents an optimal operation scheme for three networked microgrids under both normal and emergency conditions. The MGs are physically interconnected through tie-lines that remain electrically closed. Under normal operation, each MG supplies its local demand, resulting in no electrical power exchange between MGs. In addition, cyber links are established to exchange information and control signals for coordinated operation. A two-level energy management system (EMS) is designed. The lower-level EMS operates during normal conditions, while the higher-level EMS is activated during emergency conditions, such as generation deficiency or a fault leading to generation outage. For the self-healing operation, the study focuses on the final restoration stage, assuming that the fault has already been detected and isolated and that the network has reached a stable post-fault topology. At this stage, optimal power redispatch and power exchange among the interconnected MGs enable the affected microgrid to receive support from neighboring MGs and maintain the supply of the remaining connected loads. Additionally, network energy losses are considered in the optimal operation of NMGs under both normal and emergency conditions. The resultant optimization problem is addressed by applying the Pufferfish Optimization Algorithm (POA), for the first time to the best of the authors' knowledge, to the optimal operation of NMGs. Furthermore, the performance of POA is evaluated against PSO, GA, and GWO under the same computational settings, considering operating cost, network losses, computational time, and convergence behavior.

The rest of the paper is arranged as follows: The proposed EMS for the operation of NMGs is introduced in Section 2. Section 3 describes the NMGs structure. The formulation of the optimization problem is described in Section 4. Section 5 discusses the proposed POA technique. Section 6 presents the simulation results. Section 7 summarizes the main conclusions.

2. Proposed EMS for the Operation of NMG

The energy management system is an essential part in the structure of the coordinated networked microgrids system for managing the scheduling, regulation, and power flow of distributed energy resources. The proposed EMS for a framework of the NMGs considers the microturbines (MTs) acting as dispatchable sources, while the renewable energy resources (RES) operate at their available maximum power output in each hour according to available wind velocity and solar radiation. Figure 1 shows the proposed EMS for the NMGs. NMGs are linked with cyber connections for information and control signal exchange, while physical connections via tie-lines are used between MGs for electrical power exchange. The energy management framework consists of two levels, each with autonomous functions. The lower-level is designed for normal operation, where the local controller of each microgrid performs the optimal dispatch of power from the dispatchable sources. This means the NMGs are operated in a decentralized manner, where each microgrid utilizes its local resources to supply its load. When a generation deficiency or a fault leading to generation outage occurs in any MG, the higher-level EMS is activated, and the global controller is brought into operation. The MG affected by the contingency will be supported by neighboring MGs to supply the required power. The proposed management system allows each MG to operate locally under normal operating conditions. However,

during emergencies, the MGs act in coordinated operation mode, in which centralized decision-making is achieved through cooperation and information exchange among NMGs.

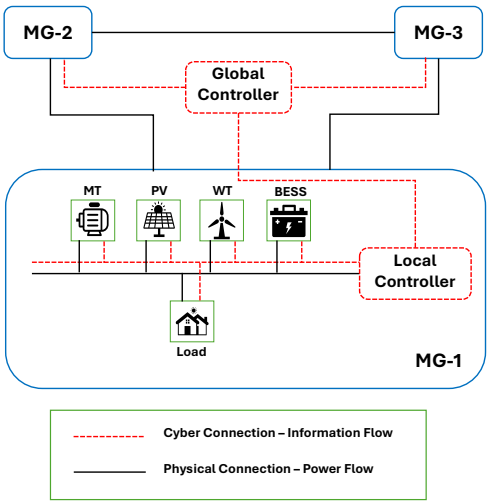


Figure 1. Proposed EMS structure.

3. The NMGs' Structure

Figure 2 shows the architecture of the proposed NMG system, which consists of three interconnected MGs. Each MG represents a modified CIGRE benchmark MG [25]. Double-circuit transmission lines are used for interconnecting the MGs. All lines are modeled using identical parameters: $R'_{ph} = 0.173\,\Omega/\text{km}$, $X'_{ph} = 0.432\,\Omega/\text{km}$, and $B'_{ph} = 3.83\,\mu\text{S/km}$. Only the line lengths are different, as shown in Table A1 in the Appendix A [26]. Cyber connections, shown in red, are used for flow of information and control signals.

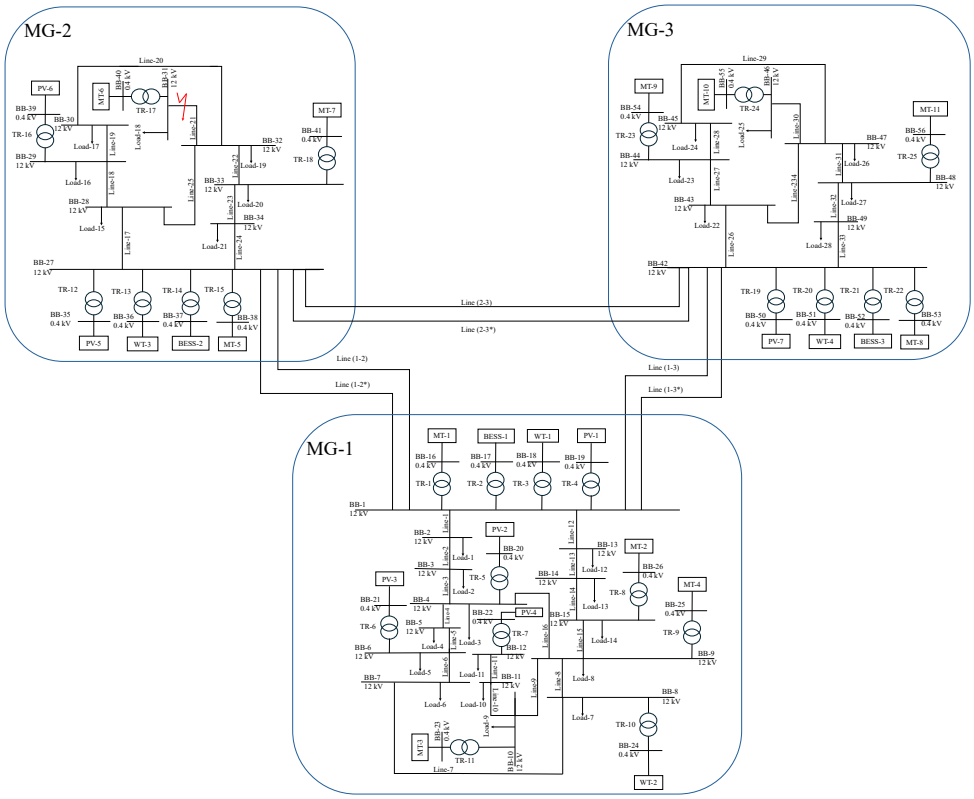


Figure 2. Networked microgrids' structure, the red arrow shows the fault location. * Parallel transmission line with the same parameters.

In this paper, the BESS operates in charging mode when the available renewable energy is greater than the total output power of the MTs. The BESS data are assumed and provided in Table A2 in the Appendix A.

3.1. Battery Energy Storage System

The battery energy storage system (BESS) is an important element in MGs, as it helps in mitigating the impact of the intermittent nature of renewable energy sources.

3.2. Micro Turbines

This research considers micro turbine generators acting as a dispatchable source. The detailed parameters of the MTs are provided in Table A3 in the Appendix A.

3.3. Power Transformers

Power transformers are used to step up the generation voltage from a low voltage level (0.4 kV) to a medium voltage level (12 kV). Table A4 in the Appendix A shows the data for power transformers [27].

3.4. Photovoltaic System Model

The hourly output of a photovoltaic (PV) module depends on the intensity of light on the PV module, ambient temperature and the PV module's characteristics. The capacity of a PV system is determined by the size of PV panels and the level of available solar radiation (SR). The solar panels are supposed to be equipped with maximum power point tracking (MPPT) controllers to extract the maximum available power. The electrical output power of the PV array is calculated using the following equation [28]:

$$P_a = \eta_a \times A \times SR(1 - 0.005\,(t_0 - 25)) \tag{1}$$

The total electrical output power of the PV system is obtained as follows:

$$P_{pv} = P_a \times N_a \tag{2}$$

The active power ratings of the PV system at each bus are assumed and presented in Table A5, while Table A6 shows the corresponding solar radiation and ambient temperature data used for the PV generation calculations [29].

3.5. Wind Turbine Model

The hourly output power of wind turbines (WTs) depends on the average hourly wind speed at the hub height and its output characteristics. Consequently, the hub height significantly affects the wind turbine generator's output power. The WT output power is calculated by converting the measured hourly average wind speed to corresponding values at the hub height. The following equation is commonly used to convert to hub heights.

$$\frac{v}{v_0} = \left(\frac{h}{h_0}\right)^{\alpha} \tag{3}$$

Generally, the value of α for an open space is taken to be 1/7 [30,31]. The output power of a wind turbine generator is modeled as a function of the wind speed and the rated power of the turbine. Accordingly, the wind turbine output power is calculated using the following expression [32]:

$$P_w = \begin{cases} 0 & if\ v_f \le v\ or\ v \le v_f \\ P_r \times \frac{v^3 - v_c^3}{v_r^3 - v_c^3} & if\ v_c \le v\ \le v_r \\ P_r & if\ v_r \le v\ \le v_f \end{cases} \quad (4)$$

The power of a specific number of wind turbines can be determined using the formula below:

$$P_{WT} = P_w \times\ N_w \times\ \eta_w \quad (5)$$

The active power ratings of the WT generators at each bus are assumed and presented in Table A5, while Table A6 shows the corresponding wind velocity data used for the WT output power calculations [29].

3.6. Daily Load Curve

The load in this study is considered as a constant P-Q load at each hour. The load at each bus is assumed to follow the same 24 h active power daily load profile multiplier, as shown in Figure 3. The peak active power demand of each load at the corresponding buses is assumed and provided in Table A7 in the Appendix A.

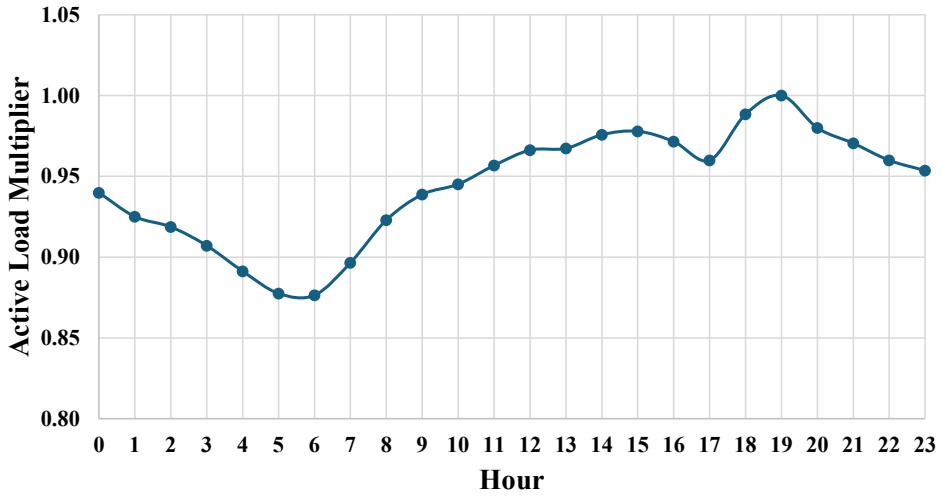


Figure 3. Active load multiplier.

4. Formulation of the Optimization Problem

The optimization problem is formulated to determine the optimal power dispatch of the NMGS while satisfying the system operating constraints. The objective function and the mathematical models of the different energy resources are presented in the following subsections.

4.1. Objective Function

The proposed optimization problem is formulated as a single-objective optimization problem. The main objective is to minimize the total operating cost of the NMGs. The total cost includes the operating costs of the MTs, WTs, PV systems and BESS together with the cost associated with network power losses. The total objective cost function is expressed as follows:

$$Min\ (total\ cost)\ =\ Min\ [MT^{cost} + WT^{cost} + PV^{cost} + BESS^{cost} + P_{Loss}^{cost}] \quad (6)$$

where the network power losses are converted into a monetary cost using the adopted loss-cost coefficient and included in the total operating cost. Therefore, network losses

are not treated as a separate optimization objective but are incorporated into the single objective function.

4.1.1. Microturbine Cost Calculation

The operating cost of the microturbines includes fuel, operation, maintenance, emission and fatigue-life costs. The fatigue rate [33] of the MTs is calculated using

$$\beta = e^{\frac{P_{out}}{P_{rated}}} \tag{7}$$

The total MT cost function is then expressed as follows:

$$MT^{cost} = \sum_{i=1}^{N_{MG}} \sum_{n=1}^{N_{MT}} \sum_{t=1}^{T} Fuel_{cost}^{MT}(t,n,I)\, OP_{cost}^{MT}(t,n,i) + MA_{cost}^{MT}(t,n,i) + EM_{cost}^{MT}(t,n,i) + FL_{cost}^{MT}(t,n,i) \tag{8}$$

The different components of the MT cost are defined by the fuel cost, operation cost, maintenance cost, emission cost and fatigue-life cost respectively, as follows:

$$Fuel_{cost}^{MT}(t,n,i) = a_i\, P_{MT}^2(t,n,i) + b_i\, P_{MT}(t,n,i) + c_i \tag{9}$$

$$OP_{cost}^{MT}(t,n,i) = P_{MT}(t,n,I) \times C_{OP}^{MT} \tag{10}$$

$$MA_{cost}^{MT}(t,n,i) = P_{MT}(t,n,I) \times C_{MA}^{MT} \tag{11}$$

$$EM_{cost}^{MT}(t,n,i) = P_{MT}(t,n,I) \times EM_{CO2}^{MT} \times Tax_{EM} \tag{12}$$

$$FL_{cost}^{MT}(t,n,i) = FL_c^{MT} \times \left[OP_{cost}^{MT}(t,n,i) + MA_{cost}^{MT}(t,n,i) + EM_{cost}^{MT}(t,n,I) \right] \times \beta_{MT} \times P_{MT}(t,n,i) \tag{13}$$

Thus, Equations (9)–(13) represent the individual cost components included in the total MT operating cost given in Equation (8).

4.1.2. Wind Turbine Cost Calculation

The total operating cost of the WTs is calculated as follows:

$$WT^{cost} = \sum_{i=1}^{N_{MG}} \sum_{n=1}^{N_{WT}} \sum_{t=1}^{T} OP_{cost}^{WT}(t,n,i) + MA_{cost}^{WT}(t,n,i) + FL_{cost}^{WT}(t,n,I) \tag{14}$$

The WT cost consists of the operation, maintenance and fatigue-life costs, which are calculated using the following equations:

$$OP_{cost}^{WT}(t,n,i) = P_{WT}(t,n,i) \times C_{OP}^{WT} \tag{15}$$

$$MA_{cost}^{WT}(t,n,i) = P_{WT}(t,n,i) \times C_{MA}^{WT} \tag{16}$$

$$FL_{cost}^{WT}(t,n,i) = FL_c^{WT} \times \left[OP_{cost}^{WT}(t,n,i) + MA_{cost}^{WT}(t,n,i) \right] \times \beta_{WT} \times P_{WT}(t,n,I) \tag{17}$$

Therefore, Equations (15)–(17) represent the individual cost components considered in the total WT cost given in Equation (14).

4.1.3. PV System Cost Calculation

The total operating cost of the PV system is calculated as follows:

$$PV^{cost} = \sum_{i=1}^{N_{MG}} \sum_{n=1}^{N_{PV}} \sum_{t=1}^{T} OP_{cost}^{PV}(t,n,i) + MA_{cost}^{PV}(t,n,i) + FL_{cost}^{PV}(t,n,I) \tag{18}$$

The corresponding operation, maintenance and fatigue-life costs of the PV system are calculated as follows:

$$OP_{cost}^{PV}(t,n,i) = \ P_{PV}(t,n,i) \ \times C_{OP}^{PV} \tag{19}$$

$$MA_{cost}^{PV}(t,n,i) = \ P_{PV}(t,n,i) \times C_{MA}^{PV} \tag{20}$$

$$FL_{cost}^{PV}(t,n,i) = FL_{c}^{PV} \ \times \left[OP_{cost}^{PV}(t,n,i) + MA_{cost}^{PV}(t,n,i)\right] \times \beta_{PV} \times P_{PV}(t,n,I) \tag{21}$$

Equations (19)–(21) represent the different cost components included in the total PV-system cost given in Equation (18).

4.1.4. BESS Cost Calculation

The total operating cost of the BESS is expressed as follows:

$$BESS^{cost} = \sum_{i=1}^{N_{MG}} \sum_{n=1}^{N_{BESS}} \sum_{t=1}^{T} \ OP_{cost}^{BESS}(t,n,i) + MA_{cost}^{BESS}(t,n,i) + \ FL_{cost}^{BESS}(t,n,I) \tag{22}$$

The BESS cost consists of the operation, maintenance and fatigue-life costs, which are calculated as follows:

$$OP_{cost}^{BESS}(t,n,i) = \ P_{BESS}(t,n,i) \ \times C_{OP}^{BESS} \tag{23}$$

$$MA_{cost}^{BESS}(t,n,i) = \ P_{BESS}(t,n,i) \times C_{MA}^{BESS} \tag{24}$$

$$FL_{cost}^{BESS}(t,n,i) = FL_{c}^{BESS} \times \left[OP_{cost}^{BESS}(t,n,i) + MA_{cost}^{BESS}(t,n,i)\right] \times \beta_{BESS} \times \ P_{BESS}(t,n,i) \tag{25}$$

Equations (23)–(25) represent the individual cost components included in the total BESS operating cost given in Equation (22).

4.2. Constraints

The optimization process is performed subject to the operational constraints of the NMGs, including the active power balance, MT generation limits, and BESS operating constraints.

4.2.1. Power Balance

For each time interval, the total generated power must satisfy the load demand and network power losses. The active power balance constraint is expressed as follows:

$$\sum P_{MT}(i,t) + \sum P_{PV}(i,t) + + \sum P_{WT}(i,t) + \sum P_{BESS} = \ \sum P_{Load}(t) \ + \ \sum P_{Loss}(t) \tag{26}$$

4.2.2. MT Limits

The output power of each MT must remain within its minimum and maximum operating limits. The MT generation constraint is defined as follows:

$$P_{MT}(min) \leq P_{MT}(i,t) \leq P_{MT}(max) \tag{27}$$

4.2.3. BESS Constraints

The BESS is operated according to the available surplus or deficit power in the NMG. The excess power equation is expressed as follows:

$$P_{excess} = \ P_{RE}(t) + P_{base} - \ P_{load}(t), \tag{28}$$

$P_{RE}(t)$ represents the total available renewable generation at time t, P_{base} represents the fixed base-generation power that is continuously available during the considered operating

period and $P_{load}(t)$ represents the load demand. The term P_{base} is a predefined constant rather than an optimization decision variable. When the sum of the renewable generation and the fixed base generation exceeds the load demand, P_{excess} becomes positive and the available surplus power can be used to charge the BESS. Conversely, when the available generation is lower than the load demand, P_{excess} becomes negative; this indicates a power deficit that can be mitigated by BESS discharging, subject to battery operating limits and *SOC* constraints.

When $P_{excess} > 0$ and $SOC(I,t) < SOC_{max}$, the BESS operates in charging mode. In this case, the charging power is limited by the available excess power and maximum *SOC*.

$$P_{BESS}(I,t) = P_{excess} \times \eta_{ch} \tag{29}$$

$$P_{BESS}(I,t) < P_{ch.max} \tag{30}$$

$$SOC(I,t) = SOC(i,t-1)\frac{P_{BESS}(i,t) \times \Delta(t) \times \eta_{ch}}{Capacity} \tag{31}$$

When $P_{excess} < 0$ and $SOC(I,t) > SOC_{min}$, the BESS operates in discharging mode, with the discharging power limited by the power deficit and the minimum *SOC*.

$$P_{BESS}(i,t) = \frac{P_{dch.max}}{\eta_{dch}} \tag{32}$$

$$SOC(i,t) = SOC(i,t-1)\frac{P_{BESS}(i,t) \times \Delta(t)}{\eta_{dch} \times Capacity} \tag{33}$$

$$SOC_{min} \leq SOC(i,t) \leq SOC_{max} \tag{34}$$

Accordingly, negative $P_{BESS}(i,t)$ represents charging, whereas positive $P_{BESS}(i,t)$ represents discharging. In this study, the initial *SOC* is set to 30%. Therefore, SOC_{min} and SOC_{max} are defined as 30% and 100%, respectively. Thus, the BESS is not allowed to discharge when the *SOC* reaches its minimum limit of 30%. Both the charging and discharging efficiencies are assumed to be 95%. The final *SOC* is not predefined; it is determined by the charging and discharging operation throughout the scheduling period while satisfying the *SOC* limits. Therefore, no terminal *SOC* constraint is imposed at the end of the scheduling horizon.

4.3. Grid Losses

Grid power losses in transmission lines and power transformers are calculated using the B-matrix loss formulation, where the total active power losses are a quadratic function of the active power injections [34]. The B-matrix coefficients are calculated based on the electrical parameters of the network, which include the transmission lines and power transformers. B, B_0, and B_{00} are the quadratic, linear and constant terms of the system loss model, respectively.

4.3.1. B-Matrix of MG-1

$$B = \begin{bmatrix} 0.0041 & -0.0002 & -0.0008 & 0.0016 \\ -0.0003 & 0.0023 & 0.0020 & -0.0001 \\ -0.0008 & 0.0020 & 0.0033 & 0.0003 \\ 0.0009 & 0.0001 & 0.0003 & 0.0057 \end{bmatrix}$$

$$B_0 = \begin{bmatrix} -0.0011 & 0.00010.0005 & 0.0020 \end{bmatrix}$$

$$B_{00} = [0.0067]$$

4.3.2. B-Matrix of MG-2

$$B = \begin{bmatrix} 0.0007 & 0.0006 & -0.0001 \\ -0.0005 & 0.0038 & -0.0012 \\ -0.0001 & -0.0009 & 0.0007 \end{bmatrix}$$

$$B_0 = \begin{bmatrix} 0.0001 & -0.0001 & 0.0001 \end{bmatrix}$$

$$B_{00} = [0.0004]$$

4.3.3. B-Matrix of MG-3

$$B = \begin{bmatrix} 0.0028 & -0.0007 & -0.0009 & 0.0008 \\ -0.0007 & -0.0008 & 0.0013 & 0.0009 \\ -0.0010 & 0.0013 & 0.0015 & -0.0027 \\ 0.0006 & 0.0007 & -0.0004 & 0.0017 \end{bmatrix}$$

$$B_0 = \begin{bmatrix} 0.0001 & 0.0007 & 0.0004 & -0.0001 \end{bmatrix}$$

$$B_{00} = [0.0042]$$

$$P_{Loss}^{cost} = \sum_{i=1}^{N_{MG}} \sum_{t=1}^{T} P_{Loss}(t, I) \times C_{Loss} \tag{35}$$

$$P_{Loss}(n,i) = \sum_{i=1}^{N_{MG}} \sum_{n=1}^{N_{MT}} \sum_{t=1}^{T} P^T(t,n,i) \times B(n,i) \times P(t,n,i) + P^T(t,n,i) \times B_0(n,i) + B_{00}(n,i) \tag{36}$$

Equation (35) is used to calculate the cost of grid losses, while the power losses themselves are calculated according to (36) as a function of B-matrix and active power injected into the grid. In this formulation, P^T denotes the transpose of the active power matrix.

5. Pufferfish Optimization Algorithm (POA)

Pufferfish belong to the family of Tetraodontidae and order Tetraodontiformes, which are usually found in marine and estuarine environments. These fish are similar to porcupinefish; however, unlike porcupinefish, which possess massive external spines, pufferfish generally have much smaller, hidden spines that only appear when inflated. Pufferfish are usually modest or medium in size, and they could not exceed 50 cm [35] in length. Pufferfish are very slow and therefore easy prey to predators. A pufferfish defends itself against predators by inflating its stomach with water, transforming into a large, spiky ball. This defense mechanism poses a significant challenge to predators seeking a quick meal, as the sharp spines make the fish difficult to swallow. Consequently, predators are generally aware of this danger and actively avoid them. Figure 4 shows the flow chart for implementing the POA. The optimization has two phases: namely, (i) Exploration (Predator Attack towards Pufferfish) and (ii) Exploitation (Defense Mechanism of Pufferfish against Predators).

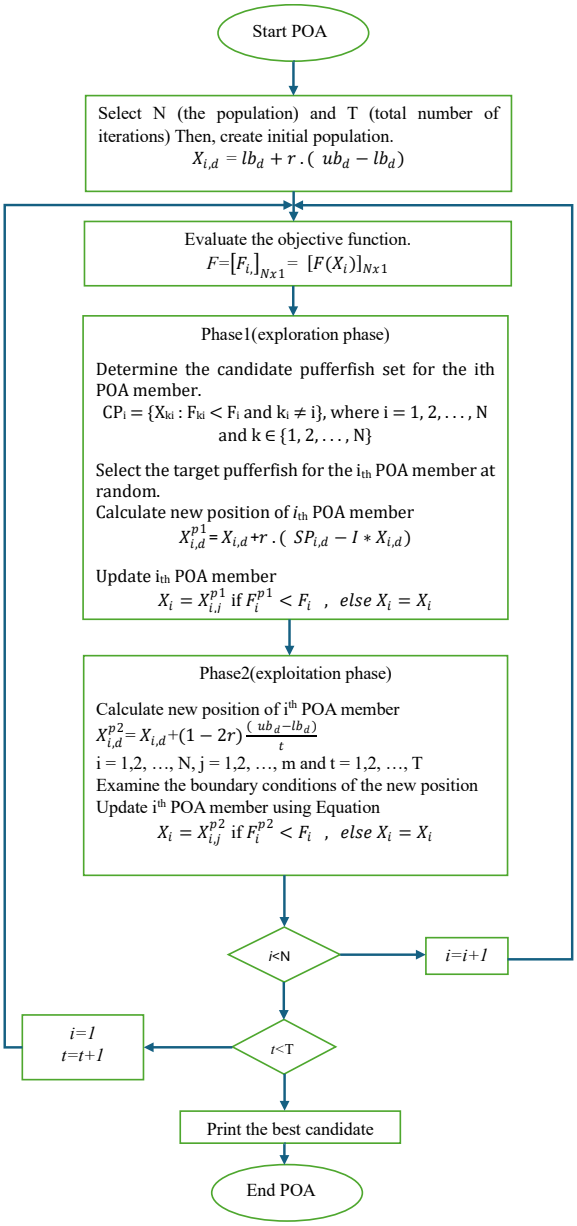


Figure 4. Flow chart of POA algorithm.

5.1. Initialization and Objective Function Evaluation

At the beginning of the optimization process, a population of N candidate solutions is generated randomly within the lower and upper bounds of the decision variables. Each candidate solution represents a possible operating point of the considered NMG economic dispatch problem. The initial position of the *ith* candidate solution is calculated as:

$$X_{i,j} = lb_j + r(ub_j - lb_j) \tag{37}$$

$X_{i,j}$ is the *jth* decision variable of the *ith* population member, lb_j and ub_j are the corresponding lower and upper bounds, respectively, and r is a random number in the interval [0,1]. After initialization, the objective function is evaluated for all population members as

$$\mathrm{F} = [F_1, \ldots, F_n]^T = [F(X_1), \ldots, F(X_n)]^T \tag{38}$$

F_i is the fitness value of the *ith* candidate solution. For the proposed NMG application, the fitness value is determined using the total operating cost defined in Equation (6). Since

the optimization problem is formulated as a minimization problem, a lower fitness value represents a better dispatch solution.

5.2. Phase 1: Exploration

The first phase of POA represents the predator attack toward the pufferfish and provides the global exploration capability of the algorithm. For each population member, a candidate pufferfish set is formed from the population members that have a better objective-function value than the current member:

$$CP_i = \{X_{ki}{:}F_{ki} < F_i, \quad k \neq i\} \tag{39}$$

CP_i denotes the candidate pufferfish set for the ith POA member. A target pufferfish SP_i is then selected randomly from CP_i. The new position of the *ith* member in the *dth* dimension is generated according to

$$X_{i,d}{}^{P1} = X_{i,d} + r.(SP_{i,d} - I \times X_{i,d}) \tag{40}$$

$X_{i,d}{}^{P1}$ is the new position generated during the exploration phase, $SP_{i,d}$ is the selected target pufferfish, r is a random number in [0,1] and I is an integer randomly selected number as 1 or 2. This mechanism enables the population to explore different regions of the search space. The newly generated position is accepted only when it improves the objective-function value according to the following greedy selection rule:

$$X_i = X_{i,j}{}^{P1} \quad \text{if } F_i{}^{P1} < F_i\text{; otherwise } X_i \text{ remains unchanged} \tag{41}$$

This exploration mechanism allows POA to investigate different candidate operating points and reduces the possibility of premature convergence to an unfavorable local solution.

5.3. Phase 2: Exploitation

The second phase represents the defense mechanism of the pufferfish and is responsible for local exploitation around the current candidate solutions. The new position of each POA member is calculated as follows:

$$X_{i,d}{}^{P2} = X_{i,d} + (1 - 2r)((ub_d - lb_d)/t) \tag{42}$$

$X_{i,d}{}^{P2}$ is the new position during the exploitation phase, ub_d and lb_d are the upper and lower bounds of the *dth* decision variable respectively, and t is the current iteration number. At the beginning of the optimization, the search step is relatively large. As t increases, the term $(ub_d - lb_d)$/t decreases, resulting in smaller local adjustments and progressively finer exploitation around the promising solutions. After checking the boundary conditions, the newly generated solution is evaluated and accepted only if it improves the fitness value:

$$X_i = X_{i,j}{}^{P2} \text{ if } F_i{}^{P2} < F_i\text{; otherwise } X_i \text{ remains unchanged} \tag{43}$$

The sequential use of the exploration and exploitation phases provides a balance between searching different regions of the solution space and refining promising dispatch solutions.

5.4. Comparative Optimization Framework

In the proposed energy management system, POA is used as the optimization engine for solving the economic dispatch problem of the interconnected NMGs. Each candidate

solution represents a possible dispatch of the controllable generation units over the considered scheduling period. Renewable generation is determined from the available PV and wind profiles, while the BESS operates according to the surplus/deficit power and *SOC* model.

To evaluate the performance of POA for the considered NMG economic dispatch problem, its performance is compared with three established metaheuristic optimization algorithms: PSO, GA, and GWO. All algorithms are implemented under the same computational settings to provide a consistent comparison. For all algorithms, the population size is set to 100, and the maximum number of iterations is set to 1000. The stopping criterion is reaching the maximum number of iterations. Each algorithm is independently executed ten times for each investigated case. The comparative assessment considers the obtained operating cost, convergence behavior, and run-to-run solution variability. The main optimization parameters used in the comparative study are summarized in Table 1. All compared algorithms use the same objective function, system constraints, population size and maximum number of iterations. This provides a consistent basis for evaluating the performance of POA against PSO, GA and GWO.

Table 1. Main parameters of the optimization algorithms.

Algorithm	Parameter	Value/Setting
POA	Exploration random coefficient, r1	U(0, 1)
	Integer coefficient, I	Randomly selected 1 or 2
	Exploitation random coefficient, r2	U(0, 1)
PSO	Inertia weight, w	Linear reduction from 0.9 to 0.1
	Cognitive coefficient, c1	2
	Social coefficient, c2	2
GA	Crossover probability, Pc	0.80
	Crossover type	Whole arithmetic
	Crossover coefficient, alpha	U(−0.5, 1.5)
	Mutation probability, Pm	0.05
GWO	Control parameter, a	Linearly reduction from 2 to 0
	Random coefficients	U(0, 1)

6. Simulation Results

The simulation studies are performed on a computer equipped with an Intel Core i5 (7th generation), 12 GB memory, and a 4 GB GPU by using MATLAB 2023. The Cost parameters of the distributed energy resources are adopted from [33], as shown in Table 2. Both normal operation and emergency conditions are considered in this study.

Table 2. Cost parameters of the distributed energy resources [33].

Unit Type	Parameter
MTs	$C_{OP}^{MT} = 13.12$ \$/MWh, $C_{MA}^{MT} = 12.5$ \$/MWh, $EM_{CO2}^{MT} = 760$ kg/MWh, $Tax_{EM} = 0.03$ \$/kg, $FL_c^{MT} = 0.02$
WTs	$C_{OP}^{WT} = 0.84$ \$/MWh, $C_{MA}^{WT} = 0.8$ \$/MWh, $FL_c^{WT} = 0.02$
PV units	$C_{OP}^{PV} = 0.95$ \$/MWh, $C_{MA}^{PV} = 0.9$ \$/MWh, $FL_c^{PV} = 0.02$
BESS	$C_{OP}^{BESS} = 0.95$ \$/MWh, $C_{MA}^{BESS} = 0.9$ \$/MWh, $FL_c^{BESS} = 0.02$

The following assumptions are made:

1- Each MG includes one MT operating as a base generator, supplying constant power throughout the 24 h period.

2- MTs have the same operation cost coefficient, maintenance cost coefficient and CO_2 gas emission factor.
3- WTs have the same operation cost and maintenance cost coefficients.
4- PV units have the same operation cost and maintenance cost coefficients.
5- MTs, WTs, PV units and BESS have the same fatigue life rate.

6.1. Case 1: Normal Operation

This case investigates the optimal scheduling of the three MGs over a 24 h period under normal operating conditions. Figures 5–7 show the optimal active-power schedules obtained using POA for MG-1, MG-2, and MG-3, respectively. Table 3 compares the performance of POA with PSO, GA, GWO, and the case without optimization. The without-optimization case represents conventional operation, in which the dispatchable sources operate according to predefined schedules without applying an economic optimization algorithm. The generator operating points are obtained from the load-flow analysis and are directly used to calculate the corresponding operating cost.

Compared with the case without optimization, POA reduces the total operating cost by approximately 7.91%, 4.78%, and 0.88% for MG-1, MG-2, and MG-3, respectively. Moreover, POA achieves the lowest operating cost compared to all (PSO, GA, GWO) optimization algorithms for the three MGs. The corresponding energy-loss reductions are approximately 12.12%, 4.00%, and 6.78%, respectively. These results demonstrate the favorable economic performance of POA while maintaining low energy losses under normal operating conditions.

Table 3. Summary of results for case 1.

MG No.	Factor	Without Optimization	POA	PSO	GA	GWO
MG-1	Total Cost ($) for one day	10,556.10	9720.80	9728.90	9728.20	9872.80
	Energy Losses (MWh)	0.99	0.87	0.88	0.89	0.94
MG-2	Total Cost ($) for one day	7338.81	6987.80	7013.40	7000.20	7008.70
	Energy Losses (MWh)	0.25	0.24	0.27	0.29	0.29
MG-3	Total Cost ($) for one day	8991.72	8912.80	8957.30	8922.20	9046.80
	Energy Losses (MWh)	0.59	0.55	0.55	0.57	0.56

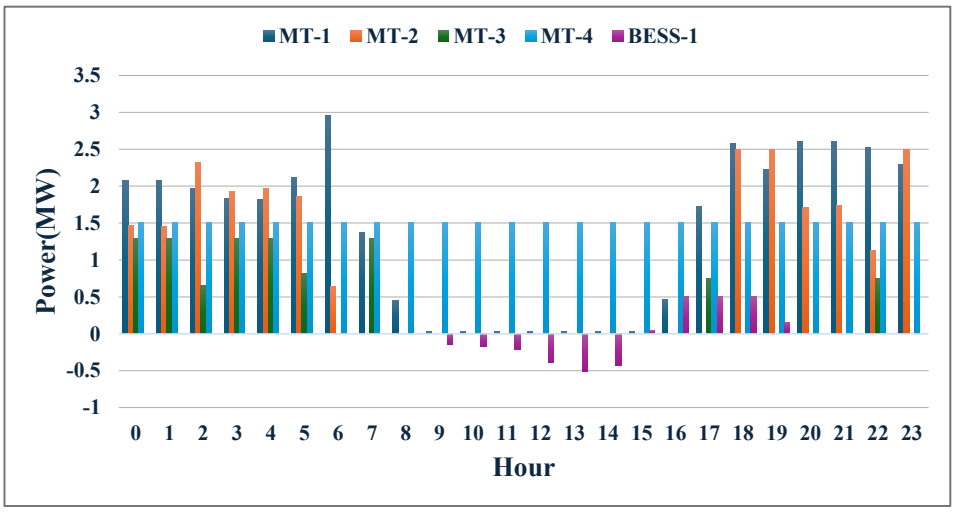


Figure 5. MTs and battery output power results for MG−1.

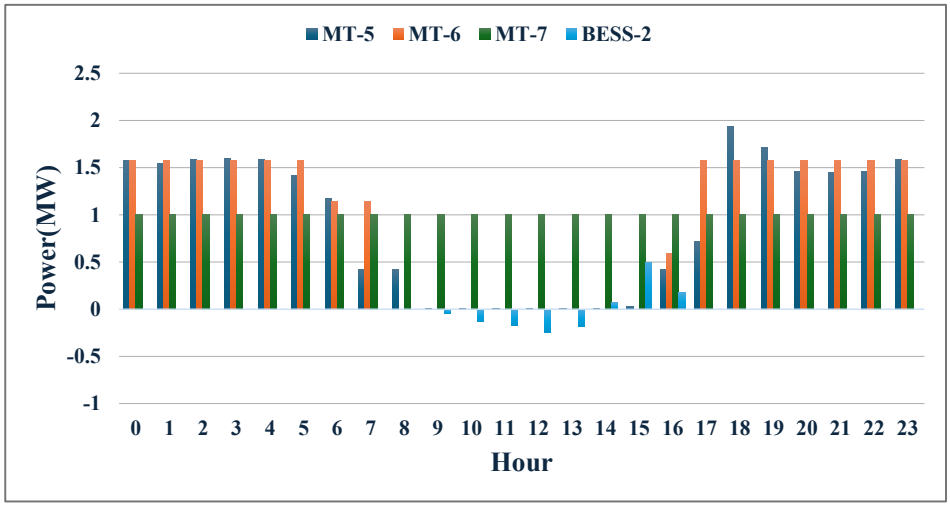


Figure 6. MTs and battery output power results for MG−2.

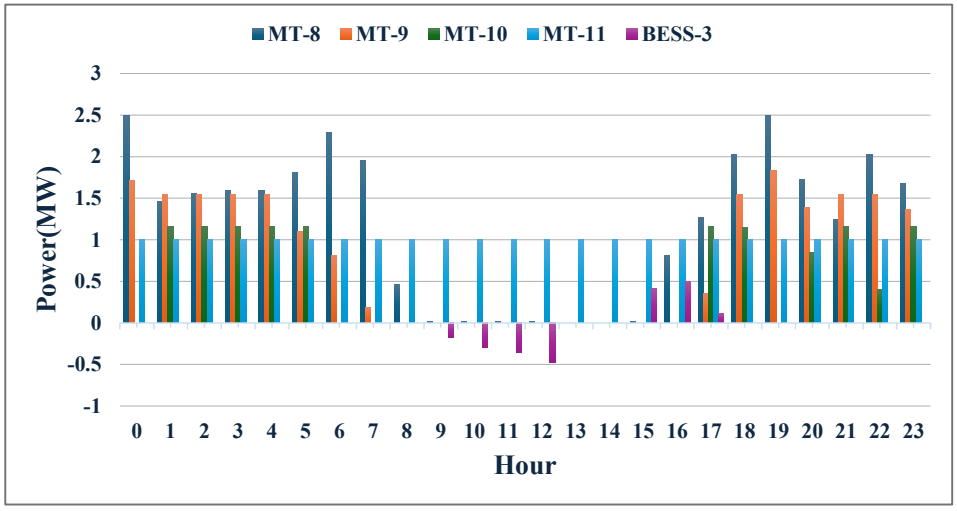


Figure 7. MTs and battery output power results for MG−3.

6.2. Case 2: Emergency Case

In emergency cases, the studies considered both generation deficiency and line fault leading to generation outage. The MG affected by emergency will receive power support from the neighboring MGs. The emergency times are selected when the output of the RES is low and the BESS is inactive in order to clearly demonstrate the influence of the NMGs under emergency conditions. Immediately after a contingency, all loads of NMGs will be supplied from all available DERs without applying the optimization algorithm to maintain the load adequacy; then, when the system reaches steady state, the optimization algorithm will redistribute the power economically among all available MTs.

6.2.1. Case 2-a: MT Outage in MG-2

In this case study, MT-5 in MG-2 is assumed to be out of service during a specified period from 8:00 p.m. to 11:00 p.m., and the analysis is performed over 3 h in steady state. MG-2 will require power support from the other MGs. At 8:00 p.m., the total load demand of MG-2 will reach 4.900 MW, while the total available power generated from the DERs in MG-2 after the outage of MT-5 will be 3.879 MW, which will not be sufficient to supply the required load demand, resulting in a power deficiency of 1.021 MW. The deficiency in power at 9:00 p.m., 10:00 p.m., and 11:00 p.m. can be calculated in the same manner,

which will be 1.013 MW, 1.019 MW, and 1.142 MW, respectively. To address this shortage, the optimization algorithm will redistribute the power economically for all available MTs. Figure 8 shows the optimal active power generation schedules for all MTs using the POA algorithm for case 2-a.

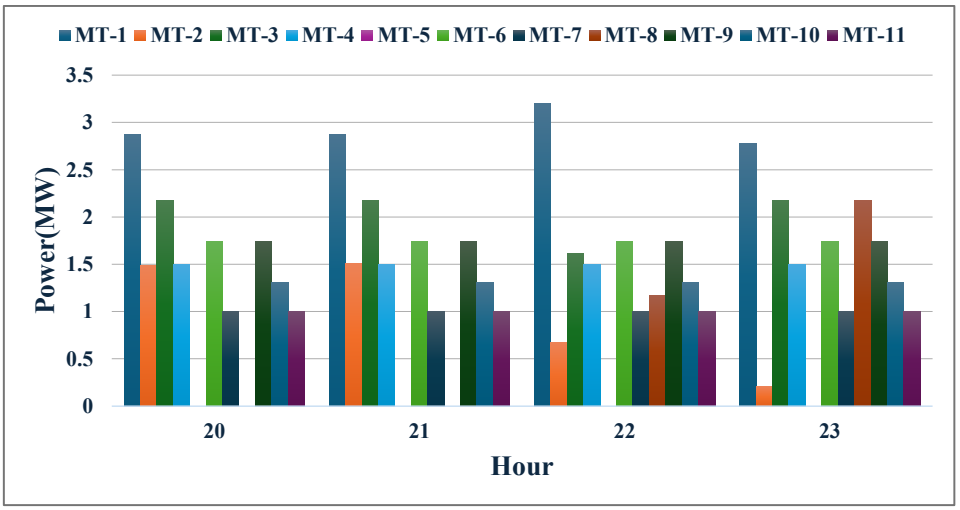


Figure 8. Case 2-a: MTs output power results by using POA.

6.2.2. Case 2-b: MT Outage in MG-2 and MG-3

In addition to the MT-5 outage in MG-2, MT-8 in MG-3 is also assumed to be out of service during the same time period. Consequently, MG-3 experiences a power deficit of 0.436 MW, 0.439 MW, 0.466 MW, and 0.677 MW at 8:00 p.m., 9:00 p.m., 10:00 p.m., and 11:00 p.m., respectively. Figure 9 shows the optimal active power generation schedules of all MTs obtained using the POA algorithm for Case 2-b.

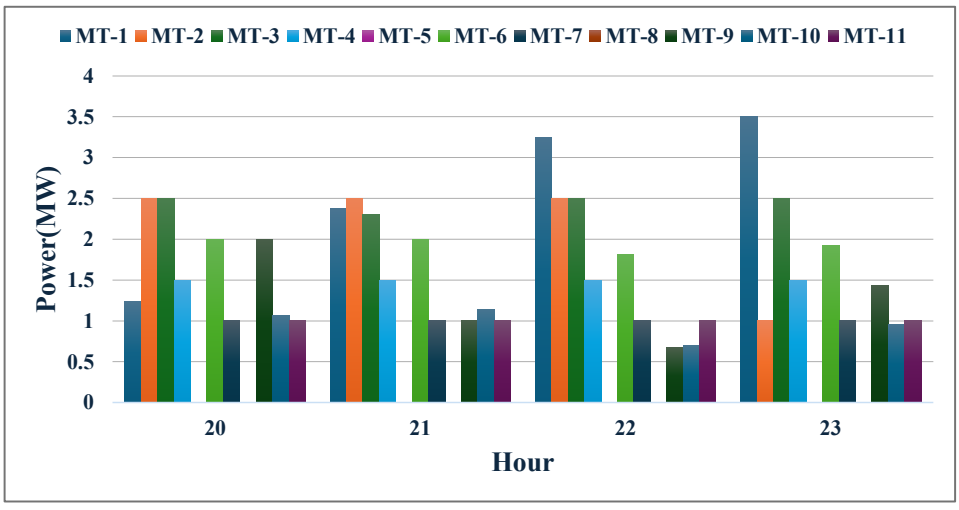


Figure 9. Case 2-b: MTs output power results by using POA.

6.2.3. Case 2-c: Line Fault Occurrence

In this case study, a fault is assumed to occur on line-21 during the specified period from 1:00 a.m. to 4:00 a.m., causing the loss of MT-6 and Load-18. Consequently, MG-2 experiences power deficiencies of 0.142 MW, 0.230 MW, 0.246 MW, and 0.242 MW at 1:00 a.m., 2:00 a.m., 3:00 a.m., and 4:00 a.m., respectively. Figure 10 shows the optimal active power generation schedules of all MTs by using the POA algorithm.

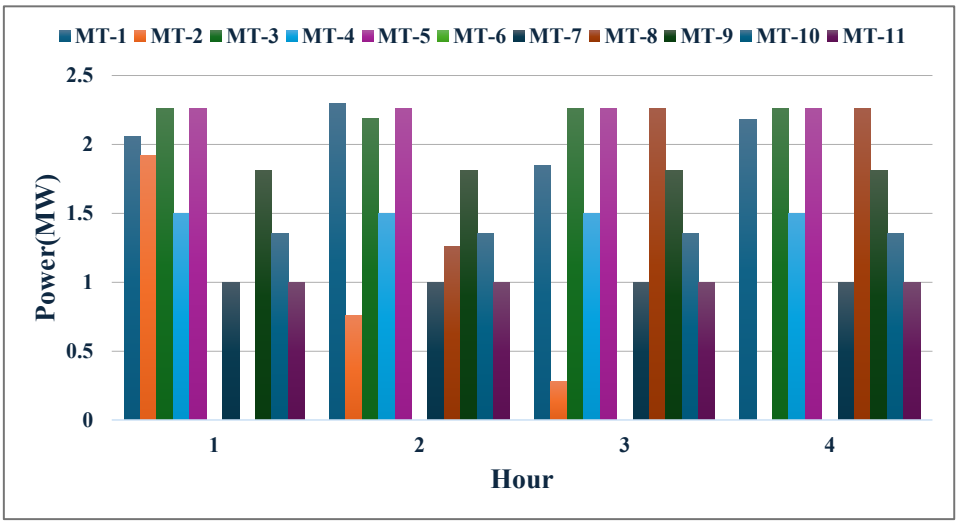


Figure 10. Case 2-c: MTs output power results by using POA.

Table 4 summarizes the total operating cost and energy losses during the outage period for Cases 2-a, 2-b, and 2-c. Compared with the case without optimization, POA reduces the operating cost by approximately 2.15%, 0.63%, and 4.33% for Cases 2-a, 2-b, and 2-c, respectively. POA also achieves the lowest operating cost among PSO, GA, and GWO in all three emergency cases. In addition, the corresponding reductions in energy losses are approximately 10.81%, 8.33%, and 35.00%, respectively. These results demonstrate the effectiveness of POA in improving the economic operation of the NMGs during emergency conditions while maintaining low energy losses.

Table 4. Summary of results for case 2.

Case No.	Factor	Without Optimization	POA	PSO	GA	GWO
Case 2-a	Total Cost ($) during outage period	5749.32	5625.90	5629.00	5636.70	5664.00
	Energy Losses (MWh) during outage period	0.37	0.33	0.34	0.35	0.35
Case 2-b	Total Cost ($) during outage period	5713.26	5677.40	5680.30	5692.5	5686.9
	Energy Losses (MWh) during outage period	0.36	0.33	0.33	0.33	0.36
Case 2-c	Total Cost ($) during outage period	5996.20	5736.40	5741.70	5743.60	5768.00
	Energy Losses (MWh) during outage period	0.20	0.13	0.13	0.13	0.16

6.3. Statistical Comparison and Convergence Analysis

To further evaluate the performance of POA, a comparative analysis is conducted against PSO, GA, and GWO for all studied cases. All algorithms are implemented using the same population size and maximum number of iterations and are independently executed ten times for each case. The comparison considers the minimum, maximum, and mean operating costs, solution variability represented by the standard deviation percentage (SD%), network losses, computational time, and convergence behavior.

Figure 11 compares the convergence characteristics of POA, PSO, GA, and GWO for all cases. The results show that POA rapidly approaches a low objective-function value and maintains favorable convergence behavior throughout the optimization process. In all cases, POA reaches the lowest final mean objective-function value compared with the other algorithms.

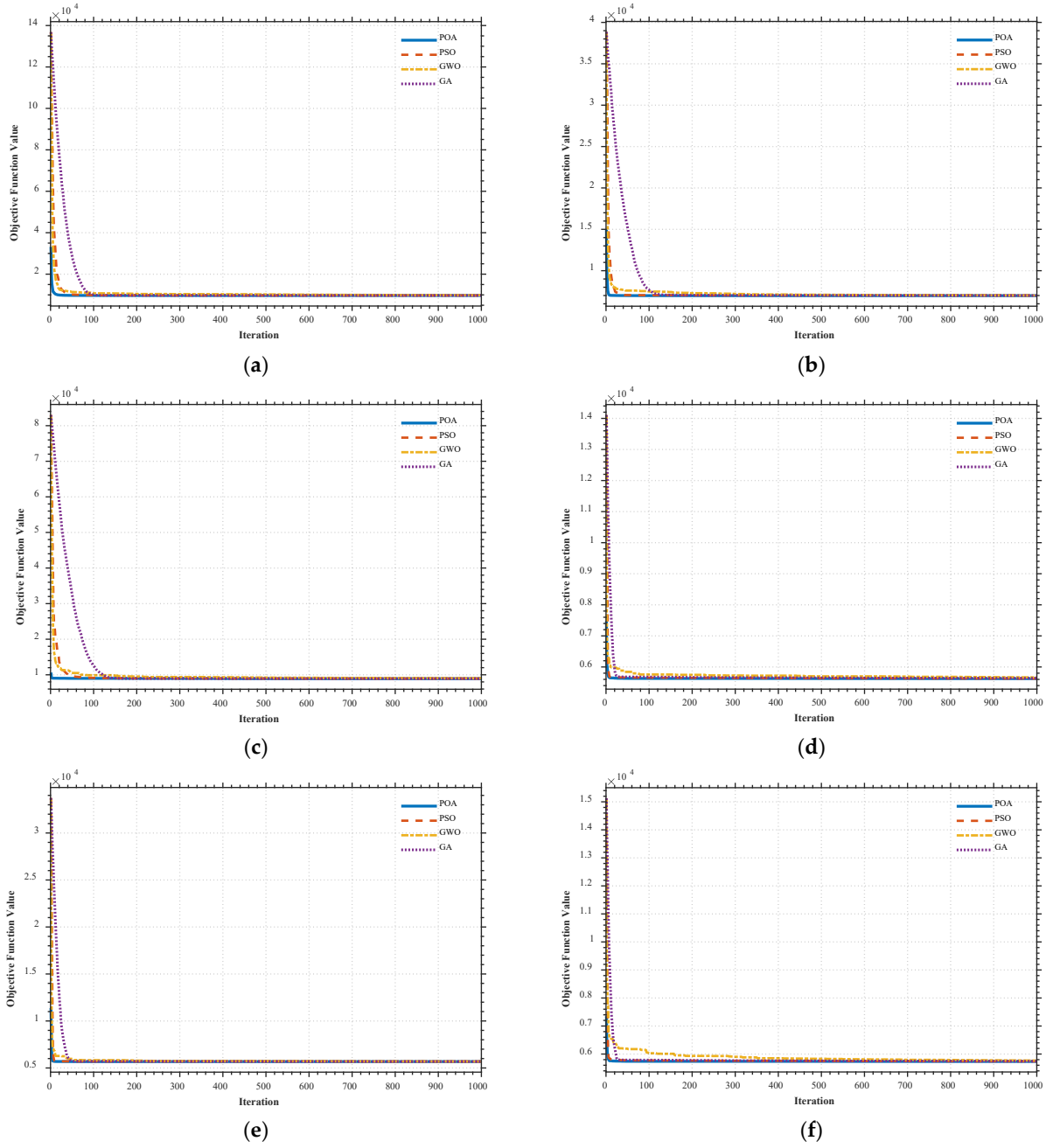


Figure 11. Convergence characteristics of POA, PSO, GA, and GWO for the investigated cases: (**a**) Case 1–MG1, (**b**) Case 1–MG2, (**c**) Case 1–MG3, (**d**) Case 2-a, (**e**) Case 2-b, and (**f**) Case 2-c.

Table 5 presents the statistical performance comparison of POA, PSO, GA, and GWO over ten independent runs for all studied cases. The results show that POA consistently achieves the lowest mean operating cost across all cases, indicating its superior economic performance under the considered operating conditions. In addition, POA exhibits low SD values, indicating good run-to-run consistency and low solution variability. The network losses obtained using POA are either the lowest or comparable to those obtained by the benchmark algorithms. Regarding computational time, POA generally requires a slightly higher execution time than the other algorithms; however, the difference remains acceptable for the considered steady-state economic dispatch problem. Overall, the results indicate a favorable trade-off between solution quality, solution consistency, and computational effort, with POA providing the best overall economic performance under the adopted simulation settings.

Table 5. Performance comparison of POA, PSO, GA, and GWO for all investigated cases.

Case No	Optimization	Min Cost	Max Cost	Mean Cost	SD (%)	Losses (MW)	Mean Time (s/run) + SD
Case1-MG1	POA	9718.20	9724.40	9720.80	0.03	0.87	4.12 ± 0.41
	PSO	9724.50	9737.40	9728.90	0.08	0.88	3.86 ± 0.51
	GA	9719.00	9737.60	9728.20	0.10	0.89	3.61 ± 0.81
	GWO	9851.50	9914.10	9872.80	0.36	0.94	3.47 ± 0.24
Case1-MG2	POA	6986.10	6990.80	6987.80	0.04	0.24	3.71 ± 0.27
	PSO	7005.60	7017.70	7013.40	0.10	0.27	2.83 ± 0.45
	GA	6992.40	7006.60	7000.20	0.10	0.29	2.53 ± 0.09
	GWO	6991.80	7037.90	7008.70	0.36	0.29	2.75 ± 0.15
Case1-MG3	POA	8910.40	8916.10	8912.80	0.03	0.55	3.82 ± 0.34
	PSO	8933.30	8974.00	8957.30	0.24	0.55	3.63 ± 0.42
	GA	8916.00	8930.40	8922.20	0.08	0.57	3.60 ± 0.22
	GWO	9036.00	9055.60	9046.80	0.11	0.56	3.93 ± 0.17
Case 2-a	POA	5625.70	5626.10	5625.90	0.01	0.33	2.91 ± 0.14
	PSO	5626.90	5631.60	5629.00	0.04	0.34	2.61 ± 0.32
	GA	5632.30	5640.40	5636.70	0.07	0.35	2.28 ± 0.87
	GWO	5638.10	5695.00	5664.00	0.51	0.35	2.30 ± 0.13
Case 2-b	POA	5677.10	5677.70	5677.40	0.01	0.33	2.09 ± 0.17
	PSO	5678.40	5682.30	5680.30	0.03	0.33	1.84 ± 0.22
	GA	5691.70	5693.00	5692.50	0.01	0.33	1.81 ± 0.26
	GWO	5684.40	5689.30	5686.90	0.04	0.36	1.89 ± 0.16
Case 2-c	POA	5735.90	5736.60	5736.40	0.01	0.13	2.48 ± 0.22
	PSO	5739.40	5743.20	5741.70	0.03	0.13	1.77 ± 0.21
	GA	5740.10	5749.90	5743.60	0.09	0.13	2.31 ± 0.74
	GWO	5750.70	5786.00	5768.00	0.31	0.16	2.07 ± 0.34

7. Conclusions

The simulation studies described in this paper have shown that the proposed POA can be effectively applied to NMGs to achieve optimal operation with reduced operating costs and energy losses under both normal and emergency conditions. In normal operation, each MG operates to minimize the operating cost and maintain self-sufficiency. The considered emergency cases leading to generation outage include generation deficiency and line fault. During emergency conditions, the affected MG receives power support from the neighboring MGs. A two-level energy management system is designed, where the lower-level EMS operates during normal conditions, while the higher-level EMS is activated during emergency conditions. The self-healing analysis focuses on the final restoration stage after fault detection and isolation, where optimal power redispatch and power exchange among the interconnected MGs are performed under a stable post-fault topology. Additionally, network energy losses are considered in the optimal operation of NMGs under both normal and emergency conditions.

The results demonstrate the effectiveness of POA in improving the economic performance of NMGs. In normal operation, the operating cost is reduced by approximately 7.91%, 4.78%, and 0.88%, while energy losses are reduced by approximately 12.12%, 4.00%, and 6.78% for MG-1, MG-2, and MG-3, respectively, compared with the case without optimization. During emergency conditions, POA reduces the operating cost by approximately 2.15%, 0.63%, and 4.33%, while energy losses are reduced by approximately 10.81%, 8.33%, and 35.00% for Cases 2-a, 2-b, and 2-c, respectively. Furthermore, comparison with PSO, GA, and GWO under the same computational settings shows that POA achieves the lowest mean operating cost across all study cases. The statistical and convergence analyses

also demonstrate low run-to-run variability and favorable convergence behavior of POA. Although POA requires slightly higher computational time than some of the benchmark algorithms, the computational differences remain relatively small, indicating a favorable trade-off between solution quality and computational effort. Also, the results highlight the capability of the networked microgrids to enhance system resilience while simultaneously improving economic performance.

Author Contributions: Conceptualization, O.H.A.; methodology, A.A.A., M.H.A. and O.H.A.; software, A.A.A.; validation, O.H.A., A.A.A. and M.H.A.; formal analysis, O.H.A. and M.H.A.; investigation, A.A.A.; resources, O.H.A. and M.H.A.; data curation, A.A.A.; writing—original draft preparation, A.A.A.; writing—review and editing, O.H.A. and M.H.A.; visualization, O.H.A. and A.A.A.; supervision, O.H.A. and M.H.A.; project administration, O.H.A. All authors have read and agreed to the published version of the manuscript.

Funding: This research received no external funding.

Institutional Review Board Statement: Not applicable.

Informed Consent Statement: Not applicable.

Data Availability Statement: The data supporting the findings of this study are included within this article. Further inquiries can be directed to the corresponding author.

Conflicts of Interest: The authors declare no conflicts of interest.

Nomenclature

Functions

EM_{cost}	Emission cost
$Fuel_{cost}$	Fuel cost
FL_{cost}	Fatigue life cost
MA_{cost}	Maintenance cost
OP_{cost}	Operation cost

Parameters

A	Area of PV Array
B	Quadratic term of B-matrix
B_0	Linear term of B-matrix
B_{00}	Constant terms of B-matrix
C_{FL}	Coefficient of fatigue life cost ($/MWh)
C_{MA}	Coefficient of maintenance cost ($/MWh)
C_{OP}	Coefficient of operation cost ($/MWh)
EM_{CO2}	CO_2 gas emission factor (kg/MWh)
FL_C	Fatigue life coefficient
N_{BESS}	Total number of BESS
N_{MG}	Total number of MGs
N_{MT}	Total number of MTs
N_{PV}	Total number of PV panels
N_{WT}	Total number of WTs
N_w	Number of wind units
Pa	Power of PV array (kW)
P_{base}	Base power (MW)
P_{BESS}	Power of BESS (MW)
P_{excess}	Excess power (MW)
P_{Load}	Load demand power (MW)
P_{Loss}	Power losses (MW)
P_{MT}	Power output of MT (MW)

P_{PV}	Power output of PV system (MW)
P_{RE}	Renewable energy power (MW)
P_r	Rated power of WT (kW)
P_{WT}	Power output of WT (MW)
SOC	State of charge of BESS (%)
SOC_{max}	Maximum state of charge (%)
SOC_{min}	Minimum state of charge (%)
SR	Solar radiation (W/m^2)
Tax_{EM}	Penalty for emission gases ($/kg)
R_{down}	Ramp-down limit (MW)
R_{up}	Ramp-up limit (MW)
ai, bi, ci	Fuel cost coefficients ($/MWh)
h_o	Reference height (m)
v	Actual wind velocity (m/s)
v_c	Cut-in wind velocity (m/s)
v_f	Cut-off wind velocity (m/s)
v_r	Rated wind velocity (m/s)
α	Coefficient of friction at the ground surface
β	Fatigue rate
Δt	Time step duration (s)
η_a	PV array conversion efficiency (%)
η_w	Wind turbine efficiency (%)
η_{BESS}^{ch}	BESS charging efficiency (%)
η_{BESS}^{dch}	BESS discharging efficiency (%).

Appendix A

Table A1. Line lengths [26].

Line No	Length (km)	Line No	Length (km)	Line No	Length (km)	Line No	Length (km)
Line-1	1.100	Line-11	0.330	Line-21	0.320	Line-31	4.890
Line-2	1.200	Line-12	1.100	Line-22	4.890	Line-32	3.550
Line-3	1.000	Line-13	4.890	Line-23	3.550	Line-33	1.100
Line-4	0.610	Line-14	2.990	Line-24	1.100	Line-34	1.000
Line-5	0.560	Line-15	1.300	Line-25	1.000	Line-(1-2)	3.000
Line-6	1.540	Line-16	0.560	Line-26	3.300	Line-(1-3)	3.000
Line-7	0.240	Line-17	3.300	Line-27	1.610	Line-(2-3)	3.000
Line-8	1.670	Line-18	1.610	Line-28	1.540		
Line-9	0.320	Line-19	1.540	Line-29	0.240		
Line-10	0.770	Line-20	0.240	Line-30	0.320		

Table A2. BESS data.

Type	Capacity (MWh)	$P_{ch.max}$ (MW)	$P_{dch.max}$ (MW)	$\eta_{ch\&dch}$ (%)	SOC_{max} (%)	SOC_{min} (%)	Bus NO
BESS-1	2.5	1.5	0.8	95	100	30	17
BESS-2	1.5	1.0	0.5	95	100	30	37
BESS-3	1.5	1.0	0.5	95	100	30	52

Table A3. MT data [9].

Type	a ($/MW^2)	b ($/MW)	c ($)	P_{max}(MW)	Type	a ($/MW^2)	b ($/MW)	c ($)	P_{max}
MT-1	0.0500	25.000	15.000	3.5	MT-7	0.026	29.325	18.325	2.0
MT-2	0.0650	30.122	9.922	2.5	MT-8	0.065	30.122	9.922	2.5
MT-3	0.0650	30.122	9.922	2.5	MT-9	0.026	29.325	18.325	2.0
MT-4 (Base)	0.0195	28.664	18.660	1.5	MT-10	0.035	34.188	18.320	1.5
MT-5	0.065	30.122	9.922	2.5	MT-11 (Base)	0.029	36.297	17.950	1.0
MT-6 (Base)	0.029	36.297	17.950	1.0					

Table A4. Transformer data [27].

TR No.	Rating (MVA)	No- Load Losses (kW)	Load Losses (kW)	Impedance (%)	TR No.	Rating (MVA)	No- Load Losses (kW)	Load Losses (kW)	Impedance (%)
TR-1	5.00	5.0	3.9	7.15	TR-14	2.00	2.1	1.9	6.00
TR-2	3.15	3.5	2.5	6.25	TR-15	3.15	3.5	2.5	6.25
TR-3	3.15	3.5	2.5	6.25	TR-16	3.15	3.5	2.5	6.25
TR-4	1.25	2.6	1.3	5.40	TR-17	1.25	2.6	1.3	5.40
TR-5	1.25	2.6	1.3	5.40	TR-18	2.00	2.1	1.9	6.00
TR-6	1.25	2.6	1.3	5.40	TR-19	3.15	3.5	2.5	6.25
TR-7	1.25	2.6	1.3	5.40	TR-20	3.15	3.5	2.5	6.25
TR-8	3.15	3.5	2.5	6.25	TR-21	2.00	2.1	1.9	6.00
TR-9	2.00	2.1	1.9	6.00	TR-22	3.15	3.5	2.5	6.25
TR-10	3.15	3.5	2.5	6.25	TR-23	3.15	3.5	2.5	6.25
TR-11	3.15	3.5	2.5	6.25	TR-24	1.25	2.6	1.3	5.40
TR-12	2.00	2.1	1.9	6.00	TR-25	2.00	2.1	1.9	6.00
TR-13	2.00	2.1	1.9	6.00					

Table A5. RES data.

Type	Active Power (MW)	Bus No.
PV-1	1	19
PV-2	1	20
PV-3	1	21
PV-4	1	22
WT-1	2	18
WT-2	2	24
PV-5	1.5	35
PV-6	1.5	39
WT-3	1.5	36
PV-7	2	50
WT-4	2.5	51

Table A6. Solar radiation, temperature and wind velocity data [29].

Time (h)	Radiation (W/m^2)	Temperature (°C)	Wind Velocity (m/s)
0	0.00	31.22	5.40
1	0.00	30.47	5.27
2	0.00	29.83	5.03

Table A6. *Cont.*

Time (h)	Radiation (W/m^2)	Temperature (°C)	Wind Velocity (m/s)
3	0.00	29.28	4.78
4	0.00	28.81	4.51
5	16.02	28.76	4.70
6	176.65	30.48	5.44
7	407.38	33.63	5.22
8	632.98	37.44	6.53
9	821.33	39.68	6.47
10	956.08	41.33	6.48
11	1006.10	42.51	6.53
12	1006.58	43.23	6.63
13	934.80	43.51	6.93
14	796.73	43.27	7.27
15	602.48	42.61	7.46
16	373.15	41.48	7.44
17	145.15	39.87	6.71
18	8.83	36.86	4.94
19	0.00	35.46	5.85
20	0.00	34.21	6.20
21	0.00	32.94	6.11
22	0.00	31.77	5.97
23	0.00	30.61	5.57

Table A7. Load data.

Load	Active Power (MW)	Reactive Power (MVAR)	Load	Active Power (MW)	Reactive Power (MVAR)
Load-1	0.850	0.362	Load-15	0.750	0.319
Load-2	0.550	0.234	Load-16	0.450	0.192
Load-3	0.350	0.149	Load-17	0.650	0.277
Load-4	0.850	0.362	Load-18	0.450	0.192
Load-5	1.000	0.426	Load-19	1.300	0.554
Load-6	1.000	0.426	Load-20	0.850	0.362
Load-7	0.650	0.277	Load-21	0.550	0.234
Load-8	0.350	0.149	Load-22	1.300	0.554
Load-9	0.450	0.192	Load-23	0.850	0.362
Load-10	0.650	0.277	Load-24	0.550	0.234
Load-11	0.650	0.277	Load-25	0.750	0.319
Load-12	0.300	0.128	Load-26	0.650	0.277
Load-13	0.350	0.149	Load-27	1.500	0.639
Load-14	0.250	0.106	Load-28	0.900	0.383

References

1. Farrokhabadi, M.; Lagos, D.; Wies, R.W.; Paolone, M.; Liserre, M.; Meegahapola, L.; Kabalan, M.; Hajimiragha, A.H.; Peralta, D.; Elizondo, M.A.; et al. Microgrid stability definitions, analysis, and examples. *IEEE Trans. Power Syst.* **2020**, *35*, 13–29. [CrossRef]
2. *IEEE Std 1547.4-2011*; IEEE Guide for Design, Operation, and Integration of Distributed Resource Island Systems with Electric Power Systems. IEEE: New York, NY, USA, 2011; pp. 1–54. [CrossRef]
3. Li, Z.; Shahidehpour, M.; Aminifar, F.; Alabdulwahab, A.; Al-Turki, Y. Networked microgrids for enhancing the power system resilience. *Proc. IEEE* **2017**, *105*, 1289–1310. [CrossRef]
4. Zidane, T.E.K.; Elshahed, M.; Benbouzid, M.; Alsumiri, M.; Eltamaly, M. Power systems and microgrids resilience enhancement strategies: A review. *Renew. Sustain. Energy Rev.* **2025**, *207*, 114953. [CrossRef]
5. Oliveira, D.Q.; de Souza, A.C.Z.; Santos, M.V.; Almeida, A.B.; Lopes, B.I.L.; Saavedra, O.R. A fuzzy-based approach for microgrids islanded operation. *Electr. Power Syst. Res.* **2017**, *149*, 178–189. [CrossRef]

6. Jiao, Z.; Wang, X.; Gong, H. Wide area measurement/wide area information-based control strategy to fast relieve overloads in a self-healing power grid. *IET Gener. Transm. Distrib.* **2014**, *8*, 1168–1176. [CrossRef]
7. Wang, Z.; Chen, B.; Wang, J.; Chen, C. Networked microgrids for self-healing power systems. *IEEE Trans. Smart Grid* **2016**, *7*, 310–319. [CrossRef]
8. Meenakshi, N.; Kavitha, D. Optimized self-healing of networked microgrids using differential evolution algorithm. In *2018 National Power Engineering Conference (NPEC)*; IEEE: Piscataway, NJ, USA, 2018. [CrossRef]
9. Vazinram, F.; Effatnejad, R.; Hedayati, M.; Hajihosseini, P. Decentralised self-healing model for gas and electricity distribution network. *IET Gener. Transm. Distrib.* **2019**, *13*, 4451–4463. [CrossRef]
10. Sun, W.; Ma, S.; Alvarez-Fernandez, I.; Roofegari Nejad, R.; Golshani, A. Optimal self-healing strategy for microgrid islanding. *IET Smart Grid* **2018**, *1*, 143–150. [CrossRef]
11. Moghateli, F.; Taher, S.A.; Karimi, A.; Shahidehpour, M. Consensus-based operational framework for self-healing in multi-microgrid systems. *IET Gener. Transm. Distrib.* **2020**, *14*, 3322–3331. [CrossRef]
12. Lu, J.; Su, J.; Zhao, R.; Chen, F.; Wang, Q.; Yan, W. A fast and accurate self-healing scheme for intelligent distribution networks using mixed integer linear programming. *IEEE Access* **2024**, *12*, 21586–21595. [CrossRef]
13. Ahmadi, S.E.; Rezaei, N. Reliability-oriented optimal scheduling of self-healing in multi-microgrids. In *2018 Smart Grid Conference (SGC)*; IEEE: Piscataway, NJ, USA, 2018. [CrossRef]
14. Abdalla, O.H.; Mostafa, A. Optimal number and locations of smart RMUs for self-healing distribution networks. *Int. Trans. Electr. Energy Syst.* **2022**, *2022*, 4819129. [CrossRef]
15. Wang, Y.; Lin, X.; Pedram, M. A near-optimal model-based control algorithm for households equipped with residential photovoltaic power generation and energy storage systems. *IEEE Trans. Sustain. Energy* **2016**, *7*, 77–86. [CrossRef]
16. Kim, K.-H.; Kim, Y.-J.; Lee, K.-Y. An efficient operation of microgrid using heuristic optimization techniques. In *2012 IEEE Power & Energy Society General Meeting*; IEEE: Piscataway, NJ, USA, 2012; pp. 1–8. [CrossRef]
17. Alanazi, A.; Alanazi, T.I. Multi-objective framework for optimal placement of distributed generations and switches in reconfigurable distribution networks: An improved particle swarm optimization approach. *Sustainability* **2023**, *15*, 9034. [CrossRef]
18. Ferahtia, S.; Rezk, H.; Djerioui, A.; Houari, A.; Fathy, A.; Abdelkareem, M.A. Optimal heuristic economic management strategy for microgrids based on PEM fuel cells. *Int. J. Hydrogen Energy* **2022**, *47*, 22038–22050. [CrossRef]
19. Jalalah, M.; Hua, L.-G.; Hafeez, G.; Ullah, S.; Alghamdi, H.; Belhaj, S. An application of heuristic optimization algorithm for demand response in smart grids with renewable energy. *AIMS Math.* **2024**, *9*, 14158–14185. [CrossRef]
20. Et-Taoussi, M.; Khaoula, A.; El Amrani, A. Bi-objective optimal active and reactive power flow management in grid-connected AC/DC hybrid microgrids using metaheuristic–PSO. *Clean Energy* **2023**, *7*, 1356–1380. [CrossRef]
21. Akter, A.; Zafir, M.E.I.; Dana, N.H.; Joysoyal, R.; Sarker, S.K.; Li, L.; Muyeen, S.M.; Das, S.K.; Kamwa, I. A review on microgrid optimization with meta-heuristic techniques: Scopes, trends and recommendation. *Energy Strategy Rev.* **2024**, *51*, 101298. [CrossRef]
22. Zheng, Z.; Yang, S.; Guo, Y.; Jin, X.; Wang, R. Meta-heuristic techniques in microgrid management: A survey. *Swarm Evol. Comput.* **2023**, *78*, 101256. [CrossRef]
23. Akarne, Y.; Essadki, A.; Annoukoubi, M.; Charadi, S.; Chakir, H.E. Enhanced energy management system for smart microgrids using an improved honey badger algorithm. *Results Eng.* **2025**, *28*, 107244. [CrossRef]
24. Naderi, E. Quantum-Accelerated Digital Twins for Cyber-Resilient Smart Power Systems Against False Data Injection Cyberattacks Using Bitcoin-Mining-Based Virtual Energy Storage Framework for Voltage Restoration. *Electronics* **2026**, *15*, 1894. [CrossRef]
25. Abdalla, O.H.; Mohamed, A.A.; Abdo, M.H. Optimal operation of a microgrid with Osprey Optimization Algorithm. In *2024 25th International Middle East Power Systems Conference (MEPCON)*; IEEE: Piscataway, NJ, USA, 2024. [CrossRef]
26. IEEE PES Task Force on Microgrid Stability Analysis and Modeling. *Microgrid Stability Definitions, Analysis, and Modeling*; Tech. Rep. PES-TR66; IEEE Power & Energy Society: Piscataway, NJ, USA, 2018.
27. ABB. Oil Distribution Transformer Catalogue. Available online: https://www.scribd.com/document/91601425/ABB-Oil-Distribution-Transformer-Catalogue (accessed on 15 August 2025).
28. Hong, Y.-Y.; Beltran, A.A.; Paglinawan, A.C. A robust design of maximum power point tracking using Taguchi method for stand-alone PV system. *Appl. Energy* **2018**, *211*, 50–63. [CrossRef]
29. NASA. Prediction of Worldwide Energy Resources (POWER) Data Access Viewer. Available online: https://power.larc.nasa.gov/data-access-viewer/ (accessed on 9 September 2025).
30. Rehman, S.; Al-Abbadi, N.M. Wind shear coefficients and energy yield for Dhahran, Saudi Arabia. *Renew. Energy* **2007**, *32*, 738–749. [CrossRef]
31. Farrugia, R. The wind shear exponent in a Mediterranean island climate. *Renew. Energy* **2003**, *28*, 647–653. [CrossRef]
32. Borowy, B.S.; Salameh, Z.M. Optimum photovoltaic array sizing for hybrid wind/photovoltaic energy systems. *IEEE Trans. Energy Convers.* **1994**, *9*, 482–488. [CrossRef]

33. Rashidi, R.; Hatami, A.; Moradi, M.; Liang, X. Optimal multi-microgrids energy management through information gap decision theory and tunicate swarm algorithm. *IEEE Access* **2024**, *12*, 114795–114808. [CrossRef]
34. Grainger, J.J.; Stevenson, W.D., Jr. *Power System Analysis*, 3rd ed.; McGraw-Hill: New York, NY, USA, 1994.
35. Al-Baik, O.; Alomari, S.; Alssayed, O.; Gochhait, S.; Leonova, I.; Dutta, U.; Malik, O.P.; Montazeri, Z.; Dehghani, M. Pufferfish optimization algorithm: A new bio-inspired metaheuristic algorithm for solving optimization problems. *Biomimetics* **2024**, *9*, 65. [CrossRef]

Disclaimer/Publisher's Note: The statements, opinions and data contained in all publications are solely those of the individual author(s) and contributor(s) and not of MDPI and/or the editor(s). MDPI and/or the editor(s) disclaim responsibility for any injury to people or property resulting from any ideas, methods, instructions or products referred to in the content.